

Differential Regulation of Amyloid-β Endocytic Trafficking and  
Lysosomal Degradation by Apolipoprotein E Isoforms\*

Jie Li<sup>1,2,3</sup>, Takahisa Kanekiyo<sup>3</sup>, Mitsuru Shinohara<sup>3</sup>, Yunwu Zhang<sup>1</sup>, Mary Jo LaDu<sup>4</sup>, Huaxi Xu<sup>1</sup>  
and Guojun Bu<sup>3,1,§</sup>

<sup>1</sup>From the Fujian Provincial Key Laboratory of Neurodegenerative Disease and Aging Research, Institute of Neuroscience, College of Medicine, <sup>2</sup>School of Pharmaceutical Sciences, Xiamen University, Xiamen, Fujian 361005, China

<sup>3</sup>Department of Neuroscience, Mayo Clinic, Jacksonville, FL 32224

<sup>4</sup>Department of Anatomy and Cell Biology, University of Illinois at Chicago, Chicago, IL 60612

\*Running title: *Aβ endocytic trafficking and lysosomal degradation*

<sup>§</sup>To whom correspondence should be addressed: Guojun Bu, Department of Neuroscience, Mayo Clinic, 4500 San Pablo Road, Jacksonville, FL 32224, USA, Tel.: (904)956-3419; Fax: (904)953-7370; E-mail: bu.guojun@mayo.edu

**Keywords:** Aβ; apoE; Alzheimer's disease; degradation; lysosome

**Background:** Apolipoprotein E (ApoE) regulates amyloid-β (Aβ) clearance in an isoform-dependent manner.

**Results:** Internalized Aβ traffics to lysosomal and recycling pathways. ApoE3 more efficiently promotes Aβ lysosomal trafficking and degradation than apoE4.

**Conclusion:** ApoE isoforms differentially affect Aβ lysosomal trafficking and degradation.

**Significance:** Differential effects of apoE isoforms on Aβ cellular degradation may explain why apoE4 is a risk factor for Alzheimer's disease.

#### SUMMARY

Aggregation of amyloid-β (Aβ) peptides leads to synaptic disruption and neurodegeneration in Alzheimer's disease (AD). A major Aβ clearance pathway in the brain is cellular uptake and degradation. However, how Aβ traffics through the endocytic pathway and how AD risk factors regulate this event is unclear. Here we show that the majority of endocytosed Aβ in neurons traffics through early and late endosomes to the lysosomes for degradation.

**Overexpression of Rab5 or Rab7, small GTPases that function in vesicle fusion for early and late endosomes, respectively, significantly accelerates Aβ endocytic trafficking to the lysosomes. We also found that a portion of endocytosed Aβ traffics through Rab11-positive recycling vesicles. A blockage of this Aβ recycling pathway with a constitutively active Rab11 mutant significantly accelerates cellular Aβ accumulation. Inhibition of lysosomal enzymes results in Aβ accumulation and aggregation. Importantly, apolipoprotein E (apoE) accelerates neuronal Aβ uptake, lysosomal trafficking and degradation in an isoform-dependent manner with apoE3 more efficiently facilitates Aβ trafficking and degradation than apoE4, a risk factor for AD. Taken together, our results demonstrate that Aβ endocytic trafficking to lysosomes for degradation is a major Aβ clearance pathway that is differentially regulated by apoE isoforms. A disturbance of this pathway can lead to accumulation and aggregation of cellular Aβ capable of causing neurotoxicity and seeding amyloid.**

Accumulation and aggregation of amyloid- $\beta$  (A $\beta$ ) peptides cleaved from amyloid precursor protein (APP) are likely initiating events in the pathogenesis of Alzheimer's disease (AD) (1-2). Overproduction or impaired clearance can both lead to A $\beta$  accumulation. Recent evidence indicates that late-onset AD cases, referring to those diagnosed with AD after the age 65, are likely caused by an overall impairment in A $\beta$  clearance (3). Genetically, among the three polymorphic alleles ( $\epsilon$ 2,  $\epsilon$ 3 and  $\epsilon$ 4), the  $\epsilon$ 4 allele of the apolipoprotein E (APOE) gene is the strongest genetic risk factor for late-onset AD (4-5). Although the primary function of apoE in the brain is to mediate cholesterol transport through apoE receptors, apoE is readily associated with A $\beta$  in AD brains (4). *In vivo* experiments have shown that apoE4 significantly decreases A $\beta$  clearance compared to apoE3 in amyloid model mice without affecting A $\beta$  production (6). However, how apoE isoforms differentially regulate A $\beta$  clearance is not clear.

A major A $\beta$  clearance pathway is cellular uptake by different cell types in brain parenchyma and in cerebral vasculature (4). Recent GWAS studies have also identified several endocytosis-related genes (BIN1, CD2AP, PICALM, CD33) that are closely related to the risk of AD in addition to APOE (7-9). Endocytosis, including receptor-mediated endocytosis and fluid-phase pinocytosis, is an efficient pathway by which extracellular proteins gain entry into intracellular compartments. The majority of endocytosed proteins traffic through several endocytic compartments before being delivered to lysosomes for degradation. Selected ligands can also be delivered to specialized organelles or recycled back to extracellular space. Rab GTPase family members play critical roles in mediating vesicular transport to different compartments. In particular, endocytic vesicles acquire Rab5 for their fusion with early endosomes, from where specific cargo proteins are delivered to either recycling endosomes through the function of Rab11, or transported to late endosomes/multivesicular bodies in a manner that depends on the function of Rab7

(10).

Several studies have shown that endocytosed A $\beta$  can be delivered to lysosomes (11-14); however, how A $\beta$  traffics through various endocytic compartments to reach lysosomes and what is the fate of A $\beta$  once it is delivered there are not clear. Thus, we systematically dissected the itinerary of A $\beta$  endocytic trafficking in neuronal cells using various organelle markers. We also assessed the effects of altered endocytic trafficking and function on cellular A $\beta$  distribution using both wild-type and mutant forms of Rab proteins (Rab5, Rab11 and Rab7). Effects of lysosomal enzyme inhibitors on A $\beta$  degradation and aggregation were also assessed. Finally, we compared the differential roles of apoE3 and apoE4 on A $\beta$  uptake and degradation. Our studies established a primary trafficking pathway of A $\beta$  to lysosomes for degradation, revealed a previously undefined recycling pathway through Rab11-positive compartments, and defined differential functions of apoE isoforms in regulating A $\beta$  cellular uptake and endocytic trafficking.

## EXPERIMENTAL PROCEDURES

*Reagents.* A $\beta$ 42, FAM-A $\beta$ 42 and TMR-A $\beta$ 42 were purchased from AnaSpec (Fremont, CA). A $\beta$  peptides were pretreated with trifluoroacetic acid, distilled under nitrogen, washed with 1,1,1,3,3,3-hexafluoro-2-propanol, distilled under nitrogen, stored at -20°C, and dissolved in DMSO to 200  $\mu$ M before use. A $\beta$ 42 solution was centrifuged at 17,000  $\times$  g for 30 seconds to remove aggregated A $\beta$ . Leupeptin, Pepstatin A, E-64d were purchased from Sigma (St. Louis, MO). Rabbit-anti-Rab5A antibody was purchased from Santa Cruz (Santa Cruz, CA). Rabbit anti-Rab7 and rabbit anti-Rab11 antibodies were purchased from Cell Signaling (Danvers, MA). Rat anti-LAMP1 antibody was purchased from BD Biosciences (San Jose, CA). Mouse anti-apoE antibody was purchased from Abcam (Cambridge, MA). Alexa568-labeled human Transferrin (Tf), Dil-low density lipoprotein (LDL) and LysoTracker Red were purchased from Invitrogen (Carlsbad, CA). Heparin was purchased from Baxter Healthcare

Corporation (Round Lake, IL). Recombinant human apoE3 and apoE4 proteins were generously provided by Dr. Yadong Huang (Gladstone Institute, CA). GFP-Rab5-WT, Rab5-DN (S34N) and Rab5-CA (Q79L) plasmids were kindly provided by Dr. Steve Caplan (University of Nebraska, NE), GFP-Rab11-CA (Q70L) plasmid was kindly provided by Dr. Wim Annaert (VIB Center for the Biology of Disease, Belgium), GFP-Rab7-WT (Addgene plasmid 12605), Rab7-DN (T22N) (Addgene plasmid 12660), Rab11-WT (Addgene plasmid 12674) and Rab11-DN (S25N) (Addgene plasmid 12678) plasmids (15) were kindly provided by Dr. Richard Pagano (Mayo Clinic, MN) and obtained from Addgene.

*Cell culture and confocal microscopy.* Mouse neuroblastoma N2a cells were cultured in DMEM/OPTI-MEM I (1:1) (Gibco) medium supplemented with 5% fetal bovine serum (Gibco), and maintained at 37°C in humidified air containing 5% CO<sub>2</sub>. Primary cortical neurons were obtained from 17-day-old embryos of wild-type C57BL/6 mice, and grown in Neurobasal medium (Gibco) supplemented with 0.5 mM Glutamax (Gibco), 2% B27 (Gibco), and 1% Penicillin-Streptomycin (P/S) (Invitrogen), in cell culture dishes precoated with poly-D-lysine solution (100  $\mu$ g/ml). At DIV5 (5 days in vitro), neurons were treated with 10  $\mu$ M cytosine arabinofuranoside (Sigma) for 2 days to remove glial cells, and media was changed to fresh Neurobasal medium containing B27 and P/S at DIV7. In some experiments, cells were cultured on 8-well chambered cover glasses (Nalge Nunc International, Rochester, NY) and observed by confocal laser-scanning fluorescence microscope (model LSM 510 invert; Carl Zeiss, Jena, Germany). The pinhole size was set to 1 AU (Airy Unit). Co-localization in the images was quantified by ImageJ software (NIH) and the Manders' coefficient was calculated with JACoP (<http://rsbweb.nih.gov/ij/plugins/track/jacop.html>).

*Transfection of Rab plasmids.* N2a cells were transfected with plasmids using Lipofectamine2000 by adding prepared

complexes directly to a suspension of cells in the plate, according to the manufacturer's instructions. Medium was changed on the following day. Cells were used 36 hours after the start of transfection.

*Detection of cell-associated A $\beta$  and apoE by ELISA.* After incubation with A $\beta$ 42 (500 nM) and/or apoE (500nM) in serum-free medium for 24 hours at 37°C, cells were harvested by incubating with trypsin for 5 minutes at 37°C. Cell pellets were collected by centrifugation at 1,000  $\times$  g for 5 minutes. After washing two times with PBS, cells were dissolved in 5 M guanidine in 50 mM Tris-HCl (pH 8.0). To measure human A $\beta$ 42, samples were captured with mAb 2.1.3 antibody, followed by detection with HRP-conjugated Ab5 antibody (16). To measure human apoE, samples were captured using AB947 antibody (Millipore), detected with biotin-conjugated goat anti-apoE antibody (Meridian Life Science) and Poly-HRP-conjugated Streptavidin (Fitzgerald). In some experiments, lysosomal inhibitors (Pepstatin A: 10  $\mu$ M, Leupeptin: 100  $\mu$ M, E-64d: 50  $\mu$ M) were added during incubation with A $\beta$ 42 and/or apoE.

*In vitro amyloid seeding assay.* After incubation with A $\beta$ 42 (500 nM) in the presence of lysosomal inhibitors in serum-free medium for 24 hours at 37°C, cells were harvested by trypsin, washed twice with PBS and homogenized in 2% SDS in PBS. *In vitro* seeding assay was performed as described previously (17). Briefly, freshly prepared TMR-A $\beta$ 42 (100 nM) was incubated with cell homogenates on 8-well chambered cover glasses for 48 hours, and amyloid aggregates were observed using a confocal microscope. For each chamber, the fluorescence intensity of A $\beta$  aggregates in 9 randomly selected fields (140  $\mu$ m  $\times$  140  $\mu$ m) was quantified by ImageJ software.

*Fluorescence-activated cell sorter (FACS)-based binding assay.* Cells were plated onto 12-well plates and allowed to grow to 90% confluency, then detached from the plates using Cell Dissociation Solution (Sigma), and incubated with FAM-A $\beta$ 42 (2  $\mu$ M), together with vehicle control, recombinant apoE3 or

apoE4 protein (500 nM) in the presence or absence of heparin (30U/ml) at 4°C for 2 hours in PBS with 1.5% heat-inactivated FBS and 0.1% sodium azide. Then cells were washed twice with PBS/FBS. Samples ( $1 \times 10^4$  cells/sample) were analyzed for fluorescence on a BD FACS Calibur (BD Biosciences). Control cells without any exposure to fluorescence were used to assess background fluorescence.

*Statistical analysis.* All quantified data represents an average of triplicate samples. Statistical significance was determined by Student's *t* test, and  $p < 0.05$  was considered significant.

## RESULTS

*Aβ traffics through Rab5- and Rab7-positive endosomal compartments.* To assess Aβ endocytic trafficking, we examined the cellular localization of TMR-Aβ42 in N2a cells transiently transfected with GFP vector control, GFP-Rab5-WT, a GFP-Rab5-dominant negative mutant (Rab5-DN, S34N), or a GFP-Rab5-constitutively active mutant (Rab5-CA, Q79L). After 24 hour incubation of cells with TMR-Aβ42,  $6.3 \pm 1.1\%$  of Aβ was co-localized with Rab5-WT-positive early endosomes (Fig. 1A, B). Aβ42 was more diffusely distributed and less co-localized with Rab5-DN mutant ( $0.4 \pm 0.2\%$ ) (Fig. 1A, B). In case of Rab5-CA mutant, Aβ42 was accumulated in Rab5-CA-positive compartments, in particular in enlarged endosomes. The co-localization of Aβ42 was higher in Rab5-CA-positive compartments ( $15.1 \pm 1.8\%$ ) (Fig. 1A, B) compared to Rab5-WT. When the amounts of cell-associated Aβ42 were quantified by ELISA after 24 hour incubation with native, unlabeled Aβ42, expression of Rab5-DN and Rab5-CA, but not Rab5-WT, significantly increased cell-associated Aβ42 compared with control (Fig. 1C). To further define Aβ42 endocytic trafficking, we used similar approaches to assess the trafficking of Alexa568-conjugated transferrin (Tf), which traffics through early and recycling endosomes. Compared with Aβ42, more Tf was detected in Rab5-WT-positive compartments ( $48.2 \pm 6.8\%$ ) (Fig. 1D, E). Tf was also captured in Rab5-CA-positive

compartments ( $59.2 \pm 6.5\%$ ) (Fig. 1D, E). Similar to Aβ42, expression of Rab5-DN mutant decreased Tf co-localization in these compartments ( $6.4 \pm 1.6\%$ ) (Fig. 1D, E). These results indicate that cell-internalized Aβ42 traffics through Rab5-positive early endosomes. A disturbance of endosomal functions, as observed in AD brains (18-19), will likely lead to Aβ42 accumulation in these intracellular compartments.

Next, we analyzed effects of overexpressing GFP-fused WT or a DN mutant (T22N) of Rab7 on cellular localization of internalized Aβ42. When DiI-labeled low-density lipoprotein (LDL), which is transferred from early to late endosomes/lysosomes, was used as a control, Rab7-DN expression resulted in a disturbed trafficking of LDL (data not shown). In the case of Aβ,  $45.8 \pm 3.9\%$  of TMR-Aβ42 was co-localized with Rab7-WT-positive late endosomal compartments, indicating that Aβ traffics mainly to Rab7-positive late endosomes, whereas only  $10.4 \pm 1.6\%$  of Aβ was transferred to Rab7-DN-positive compartments. ELISA showed that expression of neither Rab7-WT ( $1.09 \pm 0.06$  fold) nor Rab7-DN ( $1.10 \pm 0.17$  fold) affected the amounts of cell-associated Aβ42 compared with control, suggesting that Aβ might traffic to other endocytic pathways when the late endocytic pathway is perturbed.

*A small portion of Aβ traffics through Rab11-positive recycling endosomes.* To investigate whether recycling endosomes participate in the endocytic trafficking of Aβ, we examined the effects of expressing GFP-fused Rab11-WT, Rab11-DN (S25N) or Rab11-CA (Q70L) mutant on Aβ42 trafficking in N2a cells (Fig. 2A, B, C). Approximately half of internalized Tf was transported into Rab11-WT-positive endosomes, whereas Rab11-CA facilitated and Rab11-DN suppressed Tf accumulation in Rab11-positive compartments (Fig. 2D, E). A small portion of internalized TMR-Aβ42 was co-localized with Rab11-WT ( $6.7 \pm 0.9\%$ ) and the expression of Rab11-CA increased this co-localization up to  $17.4 \pm 2.5\%$  (Fig. 2A, B). Negligible amount of Aβ42 was co-localized with Rab11-DN (Fig. 2A,

B). ELISA showed that cell-associated Aβ42 level was significantly increased in cells expressing Rab11-CA compared to control (Fig. 2C), confirming that some Aβ42 indeed traffics through Rab11-positive recycling endosomes. These results indicate that despite a primary endocytic trafficking pathway through early and late endosomes, a portion of cell internalized Aβ42 can traffic through the recycling endosomes.

*Internalized Aβ42 is co-localized with Rab5, Rab7, Rab11, and LAMP1 in primary neurons.* To confirm that Aβ traffics through endosomal/lysosomal pathways in neurons, we performed immunostaining with antibodies against Rab5A, Rab11, Rab7, or LAMP1 in mouse primary cultured cortical neurons after incubations with FAM-Aβ42 (500 nM) (Fig. 3). We found that Aβ42 partially co-localized with Rab5A in neurites and cell body after 1 hour incubation (Fig. 3A). After 3 hour incubation, Aβ42 was detected in Rab11- and Rab7-positive compartments (Fig. 3B, C). Finally, Aβ42 was co-localized with lysosomal marker LAMP1 in the cell body, but not in the neurites, after 24 hour incubation (Fig. 3D). These results confirm that internalized Aβ42 is transported to either the endosome/lysosome degradation pathway or the recycling pathway in neurons.

*Inhibition of lysosomal degradation increases cell-associated Aβ and accelerates the formation of Aβ aggregates.* To assess lysosomal trafficking and degradation of Aβ, we tested the effects of lysosomal inhibitors (Leupeptin, Pepstatin A and E-64d), which block lysosomal enzyme activities (20). N2a cells were transfected with Rab5-WT, Rab7-WT, Rab11-WT, or vector (control), and then incubated with Aβ42 in the presence or absence of lysosomal inhibitors for 24 hours. ELISA showed that the presence of lysosomal inhibitors significantly increased cell-associated Aβ42 under all conditions (Fig. 4A), indicating that lysosomal degradation of Aβ42 is a significant event following cellular Aβ42 uptake. Expression of Rab5-WT, Rab7-WT or Rab11-WT did not affect cell-associated Aβ42 levels in the absence of lysosomal inhibitors. However, in the presence of lysosomal inhibitors,

expression of Rab5-WT and Rab7-WT, but not Rab11-WT, further increased cell-associated Aβ42 compared to control (Fig. 4A). These results indicate that up-regulation of Rab5 or Rab7 expression enhances Aβ transport to lysosomes where Aβ is efficiently degraded. They also suggest that a disturbance of lysosomal enzyme functions could lead to intracellular Aβ accumulation.

To examine whether cell accumulated Aβ42 possesses “seeding effect” to further facilitate Aβ42 aggregation, we tested the ability of cell-associated Aβ42 to seed aggregates *in vitro*. N2a cells transfected with vector (control), Rab5-WT, Rab7-WT or Rab11-WT were incubated with Aβ42 (500 nM) in the presence of lysosomal inhibitors for 24 hours, homogenized and incubated with freshly prepared TMR-Aβ42 (100 nM) for 48 hours. When fluorescent amyloid aggregates were observed and quantified by confocal microscopy, cell lysates from Rab5-WT and Rab7-WT, but not Rab11-WT, expressing cells induced more Aβ aggregates compared to controls (Fig. 4B, C), suggesting that lysosomal accumulated Aβ42 has sufficient ability to seed amyloid aggregates.

*ApoE facilitates Aβ lysosomal trafficking and degradation in an isoform-dependent manner.* ApoE4 is a strong risk factor for AD (4). To investigate the role of apoE isoforms in neuronal Aβ endocytic trafficking, we incubated N2a cells with Aβ42, together with vehicle control, apoE3 or apoE4 for 24 hours, in the presence or absence of lysosomal inhibitors. Cell-associated Aβ42 levels were significantly increased in the presence of apoE, with apoE3 showing a greater effect than apoE4 (Fig. 5A). In the presence of lysosomal inhibitors, cell-associated Aβ42 levels were further increased by apoE3 and apoE4 (Fig. 5A), again with apoE3 having a greater effect than apoE4. When lysosomal degradation of Aβ42 was calculated by subtracting the cell-associated Aβ in the absence of inhibitors from that in the presence of inhibitors, apoE3 enhanced Aβ42 lysosomal degradation by 1.75 folds compared to apoE4 (Fig. 5B). In addition, confocal microscopy also revealed that internalized FAM-Aβ42, which was largely co-localized with

Lysotracker, was greatly increased in the presence of apoE (Fig. 5C). Upon quantification, we confirmed that the amounts of Aβ<sub>42</sub> in lysosomes were higher in apoE3 treated cells than apoE4 treated cells (Fig. 5D).

To address whether apoE isoforms differentially affect Aβ<sub>42</sub> binding to cell surface, we carried out a FACS-based binding assay in the presence or absence of apoE3 or apoE4. Both apoE isoforms enhanced Aβ<sub>42</sub> binding to the cell surface; however, apoE3 increased cell surface-bound Aβ<sub>42</sub> more than apoE4 (1.7 fold vs. 1.4 fold compared to that of control, respectively) (Fig. 6). Consistent with our previous finding that Aβ<sub>42</sub> binds to cell surface heparan sulphate proteoglycans (HSPG) (13), the differential effects of apoE isoforms on Aβ<sub>42</sub> binding were eliminated in the presence of heparin (Fig. 6). These results demonstrate that apoE facilitates Aβ<sub>42</sub> binding to cell surface HSPG in an isoform-dependent manner.

To further dissect the mechanisms underlying the effects of apoE isoforms on Aβ<sub>42</sub>, we analyzed apoE lysosomal trafficking and degradation. We found that apoE3 was transported into lysosomes and degraded more efficiently than apoE4 (Fig. 7A, B). The more efficient trafficking of apoE3 than apoE4 was confirmed by immunostaining and confocal microscopy (Fig. 7C, D). These results suggest that apoE isoforms likely facilitate Aβ<sub>42</sub> lysosomal trafficking and degradation by serving as Aβ<sub>42</sub> trafficking chaperones.

## DISCUSSION

In the brains of AD patients, Aβ deposition is more abundantly detected in APOE4 carriers than non-carriers (21-23). Although several Aβ-independent mechanisms exist, the primary pathway by which apoE4 increases the risk of AD is likely to facilitate Aβ accumulation and aggregation in the brain (24). In this study, we defined the cellular itinerary of Aβ endocytic trafficking and lysosomal degradation. More importantly, we demonstrated an apoE isoform-dependent effect on Aβ lysosomal trafficking and degradation in neuronal cells. Although both apoE3 and apoE4 facilitate cellular Aβ binding and subsequent lysosomal

trafficking and degradation, apoE3 consistently exhibits greater effects than apoE4. The differences of cell-associated Aβ between apoE3 and apoE4 were further exacerbated in the presence of lysosomal inhibitors, indicating that apoE3 possesses greater ability to accelerate lysosomal degradation of Aβ than apoE4. Recently, Castellano and colleagues have used *in vivo* microdialysis technique to demonstrate an apoE isoform-dependent Aβ clearance in PDAPP/TRE mice, with higher concentration of ISF Aβ and slower Aβ clearance rate in the hippocampus of PDAPP/E4 mice than in PDAPP/E3 mice, suggesting a lesser role of apoE4 in supporting Aβ clearance than apoE3 (6). Our *in vitro* findings demonstrating a greater ability of apoE3 to facilitate Aβ clearance than apoE4 are consistent with these *in vivo* results.

A possible mechanism by which apoE isoforms differentially accelerate Aβ cellular uptake and lysosomal trafficking is to enhance Aβ binding to cell surface receptors. Our recent work has shown that cell surface HSPG constitutes a major Aβ binding site on the neuronal cell surface (13). As apoE is also a high affinity heparin-binding protein (25), it is possible that apoE isoforms differentially affect Aβ binding to cell surface HSPG. Indeed, our results clearly show apoE3 increases Aβ binding to neuronal cell surface more than apoE4 in a manner that depends on the availability of HSPG. Whether such effects depend on a direct interaction between apoE and Aβ is not clear. Previous *in vitro* studies have demonstrated that apoE3 binds to Aβ with higher affinity than apoE4 (26-27), and native apoE3 forms a larger amount of SDS-stable complex with Aβ than apoE4 (28). Thus, it is possible that apoE3 more readily forms apoE/Aβ complexes than apoE4 and that these apoE/Aβ complexes have a greater affinity to cell surface HSPG than Aβ alone. Alternatively, binding of apoE isoforms to cell surface HSPG generates higher affinity binding sites for Aβ. Finally, binding of apoE isoforms to cell surface HSPG might alter its conformation and/or charge properties such that it is more prone to Aβ binding. Further studies are needed to address these possibilities.

Receptor-mediated endocytosis often leads

to trafficking through early/late endosomes *en route* to lysosomes for degradation as for the case of LDL and a variety of other extracellular ligands. In this work, we defined the endocytic trafficking pathway by which extracellular A $\beta$  is eventually delivered to lysosomes. We found that the majority of internalized A $\beta$  traffics through Rab5- and Rab7-positive early and late endosomes, respectively. Most internalized A $\beta$  is delivered to the lysosomal pathway for degradation. Because overexpression of Rab5 and Rab7 both accelerate A $\beta$  trafficking to lysosomes and its degradation, the endosome/lysosome route likely represents a major endocytic trafficking pathway for A $\beta$ . Interestingly, we also identified a co-localization of A $\beta$  with recycling endosome marker Rab11, albeit to a smaller extent compared to those for Rab5 and Rab7, suggesting that at least a portion of endocytosed A $\beta$  can be recycled. To our knowledge, this is the first report demonstrating a potential pathway for A $\beta$  recycling. The physiological and pathophysiological significance of this potential A $\beta$  recycling pathway is not clear.

Autophagy also plays an important role in AD pathogenesis where A $\beta$  is subsequently degraded by autophagolysosome/lysosomes (29-30). Autophagy, receptor-mediated endocytosis, and pinocytosis (fluid-phase endocytosis) converge in lysosomes where a variety of acid hydrolases, including cathepsin B and cathepsin D, serve as A $\beta$  degrading enzymes (31). These findings suggest that lysosomes have a high capacity to degrade A $\beta$  and a disturbance of this A $\beta$  degradation pathway could critically affect A $\beta$  metabolism. As high concentrations of A $\beta$  (32) and the acidic environment in the endosomal/lysosomal compartments (33) promote A $\beta$  aggregation, a disturbance of lysosomal function can lead to harmful A $\beta$  aggregation. Such a possibility is highlighted in our current study where the presence of lysosomal inhibitors leads to A $\beta$  lysosomal accumulation and aggregation. More importantly, these A $\beta$  aggregates are capable of seeding additional A $\beta$  aggregates, presenting a possibility that A $\beta$  aggregation and deposition in AD brains might be initiated within the

lysosomes. Pathological conditions such as increased A $\beta$  production and/or impaired endosomal/lysosomal functions can lead to similar A $\beta$  aggregates in the lysosomes. In addition to seeding amyloid, intracellular A $\beta$  aggregates might also be exocytosed to the extracellular environments where they injure synapses and trigger neurodegeneration. In this regard, mounting recent work has demonstrated a greater toxicity associated with soluble A $\beta$  oligomers (34-38). Whether A $\beta$  oligomers are generated intracellularly, extracellularly, or both, requires further investigation. A $\beta$  aggregates also destabilize the lysosomal membrane (39), which further compromises lysosomal function and induces leakage of hydrolases into cytoplasmic compartment, contributing to ultimate neuronal death (40-41). Several studies have shown that endosome/lysosome abnormality, including their enlargement, is often induced in early stages of AD (18-19,42-43). Furthermore, presenilin 1 (PS1) mutations, causing early-onset AD, induce a disturbed lysosomal/autophagy phenotype by affecting lysosome acidification and proteolysis (44). Together, these evidences suggest that a disturbance of lysosome functions could be the first step to induce A $\beta$  aggregation in lysosomes, which results in further damage to lysosomes, generating a vicious cycle in the pathogenesis of AD.

In summary, we have established an A $\beta$  endocytic trafficking itinerary that includes a major pathway to the lysosomes for degradation and a minor pathway to Rab11-positive compartments for recycling. We have also demonstrated that apoE facilitates A $\beta$  binding and lysosomal trafficking in an isoform-dependent manner, with apoE3 more efficiently enhances A $\beta$  trafficking and degradation than apoE4. Our work suggests a possibility that early endosome/lysosome dysfunctions likely lead to A $\beta$  intracellular accumulation and aggregation, initiating a cascade of events that ultimately cause injuries to synapses and neurons. Better understanding on apoE isoform-dependent effects on A $\beta$  metabolism might allow us to address why apoE4 is a strong risk factor for AD and how we can identify new targets for AD diagnosis and

therapy.

## REFERENCES

1. Hardy, J., and Selkoe, D. J. (2002) The amyloid hypothesis of Alzheimer's disease: progress and problems on the road to therapeutics. *Science* **297**, 353-356
2. Goedert, M., and Spillantini, M. G. (2006) A century of Alzheimer's disease. *Science* **314**, 777-781
3. Mawuenyega, K. G., Sigurdson, W., Ovod, V., Munsell, L., Kasten, T., Morris, J. C., Yarasheski, K. E., and Bateman, R. J. (2010) Decreased clearance of CNS  $\beta$ -amyloid in Alzheimer's disease. *Science* **330**, 1774
4. Bu, G. (2009) Apolipoprotein E and its receptors in Alzheimer's disease: pathways, pathogenesis and therapy. *Nat. Rev. Neurosci.* **10**, 333-344
5. Holtzman, D. M., Herz, J., and Bu, G. (2012) Apolipoprotein E and apolipoprotein E receptors: normal biology and roles in Alzheimer disease. *Cold. Spring. Harb. Perspect. Med.* **2**, a006312
6. Castellano, J. M., Kim, J., Stewart, F. R., Jiang, H., DeMattos, R. B., Patterson, B. W., Fagan, A. M., Morris, J. C., Mawuenyega, K. G., Cruchaga, C., Goate, A. M., Bales, K. R., Paul, S. M., Bateman, R. J., and Holtzman, D. M. (2011) Human apoE isoforms differentially regulate brain amyloid- $\beta$  peptide clearance. *Sci. Transl. Med.* **3**, 89ra57
7. Harold, D., Abraham, R., Hollingworth, P., Sims, R., Gerrish, A., Hamshere, M. L., Pahwa, J. S., Moskvina, V., Dowzell, K., Williams, A., Jones, N., Thomas, C., Stretton, A., Morgan, A. R., Lovestone, S., Powell, J., Proitsi, P., Lupton, M. K., Brayne, C., Rubinsztein, D. C., Gill, M., Lawlor, B., Lynch, A., Morgan, K., Brown, K. S., Passmore, P. A., Craig, D., McGuinness, B., Todd, S., Holmes, C., Mann, D., Smith, A. D., Love, S., Kehoe, P. G., Hardy, J., Mead, S., Fox, N., Rossor, M., Collinge, J., Maier, W., Jessen, F., Schurmann, B., van den Bussche, H., Heuser, I., Kornhuber, J., Wiltfang, J., Dichgans, M., Frolich, L., Hampel, H., Hull, M., Rujescu, D., Goate, A. M., Kauwe, J. S., Cruchaga, C., Nowotny, P., Morris, J. C., Mayo, K., Sleegers, K., Bettens, K., Engelborghs, S., De Deyn, P. P., Van Broeckhoven, C., Livingston, G., Bass, N. J., Gurling, H., McQuillin, A., Gwilliam, R., Deloukas, P., Al-Chalabi, A., Shaw, C. E., Tsolaki, M., Singleton, A. B., Guerreiro, R., Muhleisen, T. W., Nothen, M. M., Moebus, S., Jockel, K. H., Klopp, N., Wichmann, H. E., Carrasquillo, M. M., Pankratz, V. S., Younkin, S. G., Holmans, P. A., O'Donovan, M., Owen, M. J., and Williams, J. (2009) Genome-wide association study identifies variants at CLU and PICALM associated with Alzheimer's disease. *Nat. Genet.* **41**, 1088-1093
8. Lambert, J. C., Heath, S., Even, G., Campion, D., Sleegers, K., Hiltunen, M., Combarros, O., Zelenika, D., Bullido, M. J., Tavernier, B., Letenneur, L., Bettens, K., Berr, C., Pasquier, F., Fievet, N., Barberger-Gateau, P., Engelborghs, S., De Deyn, P., Mateo, I., Franck, A., Helisalmi, S., Porcellini, E., Hanon, O., de Pancorbo, M. M., Lendon, C., Dufouil, C., Jaillard, C., Leveillard, T., Alvarez, V., Bosco, P., Mancuso, M., Panza, F., Nacmias, B., Bossu, P., Piccardi, P., Annoni, G., Seripa, D., Galimberti, D., Hannequin, D., Licastro, F., Soininen, H., Ritchie, K., Blanche, H., Dartigues, J. F., Tzourio, C., Gut, I., Van Broeckhoven, C., Alperovitch, A., Lathrop, M., and Amouyel, P. (2009) Genome-wide association study identifies variants at CLU and CR1 associated with Alzheimer's disease. *Nat. Genet.* **41**, 1094-1099
9. Naj, A. C., Jun, G., Beecham, G. W., Wang, L. S., Vardarajan, B. N., Buross, J., Gallins, P. J., Buxbaum, J. D., Jarvik, G. P., Crane, P. K., Larson, E. B., Bird, T. D., Boeve, B. F., Graff-Radford, N. R., De Jager, P. L., Evans, D., Schneider, J. A., Carrasquillo, M. M., Ertekin-Taner, N., Younkin, S. G., Cruchaga, C., Kauwe, J. S., Nowotny, P., Kramer, P., Hardy,

- J., Huentelman, M. J., Myers, A. J., Barmada, M. M., Demirci, F. Y., Baldwin, C. T., Green, R. C., Rogaeva, E., St George-Hyslop, P., Arnold, S. E., Barber, R., Beach, T., Bigio, E. H., Bowen, J. D., Boxer, A., Burke, J. R., Cairns, N. J., Carlson, C. S., Carney, R. M., Carroll, S. L., Chui, H. C., Clark, D. G., Corneveaux, J., Cotman, C. W., Cummings, J. L., DeCarli, C., DeKosky, S. T., Diaz-Arrastia, R., Dick, M., Dickson, D. W., Ellis, W. G., Faber, K. M., Fallon, K. B., Farlow, M. R., Ferris, S., Frosch, M. P., Galasko, D. R., Ganguli, M., Gearing, M., Geschwind, D. H., Ghetti, B., Gilbert, J. R., Gilman, S., Giordani, B., Glass, J. D., Growdon, J. H., Hamilton, R. L., Harrell, L. E., Head, E., Honig, L. S., Hulette, C. M., Hyman, B. T., Jicha, G. A., Jin, L. W., Johnson, N., Karlawish, J., Karydas, A., Kaye, J. A., Kim, R., Koo, E. H., Kowall, N. W., Lah, J. J., Levey, A. I., Lieberman, A. P., Lopez, O. L., Mack, W. J., Marson, D. C., Martiniuk, F., Mash, D. C., Masliah, E., McCormick, W. C., McCurry, S. M., McDavid, A. N., McKee, A. C., Mesulam, M., Miller, B. L., Miller, C. A., Miller, J. W., Parisi, J. E., Perl, D. P., Peskind, E., Petersen, R. C., Poon, W. W., Quinn, J. F., Rajbhandary, R. A., Raskind, M., Reisberg, B., Ringman, J. M., Roberson, E. D., Rosenberg, R. N., Sano, M., Schneider, L. S., Seeley, W., Shelanski, M. L., Slifer, M. A., Smith, C. D., Sonnen, J. A., Spina, S., Stern, R. A., Tanzi, R. E., Trojanowski, J. Q., Troncoso, J. C., Van Deerlin, V. M., Vinters, H. V., Vonsattel, J. P., Weintraub, S., Welsh-Bohmer, K. A., Williamson, J., Woltjer, R. L., Cantwell, L. B., Dombroski, B. A., Beekly, D., Lunetta, K. L., Martin, E. R., Kamboh, M. I., Saykin, A. J., Reiman, E. M., Bennett, D. A., Morris, J. C., Montine, T. J., Goate, A. M., Blacker, D., Tsuang, D. W., Hakonarson, H., Kukull, W. A., Foroud, T. M., Haines, J. L., Mayeux, R., Pericak-Vance, M. A., Farrer, L. A., and Schellenberg, G. D. (2011) Common variants at MS4A4/MS4A6E, CD2AP, CD33 and EPHA1 are associated with late-onset Alzheimer's disease. *Nat. Genet.* **43**, 436-441
10. Stenmark, H. (2009) Rab GTPases as coordinators of vesicle traffic. *Nat. Rev. Mol. Cell. Biol.* **10**, 513-525
  11. Mandrekar, S., Jiang, Q., Lee, C. Y., Koenigsknecht-Talboo, J., Holtzman, D. M., and Landreth, G. E. (2009) Microglia mediate the clearance of soluble Aβ through fluid phase macropinocytosis. *J. Neurosci.* **29**, 4252-4262
  12. Fuentealba, R. A., Liu, Q., Zhang, J., Kanekiyo, T., Hu, X., Lee, J. M., LaDu, M. J., and Bu, G. (2010) Low-density lipoprotein receptor-related protein 1 (LRP1) mediates neuronal Aβ42 uptake and lysosomal trafficking. *PLoS One* **5**, e11884
  13. Kanekiyo, T., Zhang, J., Liu, Q., Liu, C. C., Zhang, L., and Bu, G. (2011) Heparan Sulphate Proteoglycan and the Low-Density Lipoprotein Receptor-Related Protein 1 Constitute Major Pathways for Neuronal Amyloid-β Uptake. *J. Neurosci.* **31**, 1644-1651
  14. Basak, J. M., Verghese, P. B., Yoon, H., Kim, J., and Holtzman, D. M. (2012) Low-density lipoprotein receptor represents an apolipoprotein E-independent pathway of Aβ uptake and degradation by astrocytes. *J. Biol. Chem.* **287**, 13959-13971
  15. Choudhury, A., Dominguez, M., Puri, V., Sharma, D. K., Narita, K., Wheatley, C. L., Marks, D. L., and Pagano, R. E. (2002) Rab proteins mediate Golgi transport of caveola-internalized glycosphingolipids and correct lipid trafficking in Niemann-Pick C cells. *J. Clin. Invest.* **109**, 1541-1550
  16. Chakrabarty, P., Ceballos-Diaz, C., Beccard, A., Janus, C., Dickson, D., Golde, T. E., and Das, P. (2010) IFN-gamma promotes complement expression and attenuates amyloid plaque deposition in amyloid β precursor protein transgenic mice. *J. Immunol.* **184**, 5333-5343
  17. Hu, X., Crick, S. L., Bu, G., Frieden, C., Pappu, R. V., and Lee, J. M. (2009) Amyloid seeds formed by cellular uptake, concentration, and aggregation of the amyloid-β peptide. *Proc. Natl. Acad. Sci.* **106**, 20324-20329
  18. Cataldo, A. M., Peterhoff, C. M., Troncoso, J. C., Gomez-Isla, T., Hyman, B. T., and Nixon, R. A. (2000) Endocytic pathway abnormalities precede amyloid β deposition in sporadic

- Alzheimer's disease and Down syndrome: differential effects of APOE genotype and presenilin mutations. *Am. J. Pathol.* **157**, 277-286
19. Cataldo, A. M., Petanceska, S., Terio, N. B., Peterhoff, C. M., Durham, R., Mercken, M., Mehta, P. D., Buxbaum, J., Haroutunian, V., and Nixon, R. A. (2004) Aβ localization in abnormal endosomes: association with earliest Aβ elevations in AD and Down syndrome. *Neurobiol. Aging*. **25**, 1263-1272
  20. Iwabu, Y., Fujita, H., Kinomoto, M., Kaneko, K., Ishizaka, Y., Tanaka, Y., Sata, T., and Tokunaga, K. (2009) HIV-1 accessory protein Vpu internalizes cell-surface BST-2/tetherin through transmembrane interactions leading to lysosomes. *J. Biol. Chem.* **284**, 35060-35072
  21. Schmechel, D. E., Saunders, A. M., Strittmatter, W. J., Crain, B. J., Hulette, C. M., Joo, S. H., Pericak-Vance, M. A., Goldgaber, D., and Roses, A. D. (1993) Increased amyloid β-peptide deposition in cerebral cortex as a consequence of apolipoprotein E genotype in late-onset Alzheimer disease. *Proc. Natl. Acad. Sci.* **90**, 9649-9653
  22. Polvikoski, T., Sulkava, R., Haltia, M., Kainulainen, K., Vuorio, A., Verkkoniemi, A., Niinisto, L., Halonen, P., and Kontula, K. (1995) Apolipoprotein E, dementia, and cortical deposition of β-amyloid protein. *N. Engl. J. Med.* **333**, 1242-1247
  23. Kok, E., Haikonen, S., Luoto, T., Huhtala, H., Goebeler, S., Haapasalo, H., and Karhunen, P. J. (2009) Apolipoprotein E-dependent accumulation of Alzheimer disease-related lesions begins in middle age. *Ann. Neurol.* **65**, 650-657
  24. Huang, Y., and Mucke, L. (2012) Alzheimer mechanisms and therapeutic strategies. *Cell* **148**, 1204-1222
  25. Mahley, R. W., and Rall, S. C., Jr. (2000) Apolipoprotein E: far more than a lipid transport protein. *Annu. Rev. Genomics. Hum. Genet.* **1**, 507-537
  26. LaDu, M. J., Falduto, M. T., Manelli, A. M., Reardon, C. A., Getz, G. S., and Frail, D. E. (1994) Isoform-specific binding of apolipoprotein E to β-amyloid. *J. Biol. Chem.* **269**, 23403-23406
  27. LaDu, M. J., Pederson, T. M., Frail, D. E., Reardon, C. A., Getz, G. S., and Falduto, M. T. (1995) Purification of apolipoprotein E attenuates isoform-specific binding to β-amyloid. *J. Biol. Chem.* **270**, 9039-9042
  28. Manelli, A. M., Stine, W. B., Van Eldik, L. J., and LaDu, M. J. (2004) ApoE and Aβ1-42 interactions: effects of isoform and conformation on structure and function. *J. Mol. Neurosci.* **23**, 235-246
  29. Nixon, R. A. (2007) Autophagy, amyloidogenesis and Alzheimer disease. *J. Cell. Sci.* **120**, 4081-4091
  30. Boland, B., Kumar, A., Lee, S., Platt, F. M., Wegiel, J., Yu, W. H., and Nixon, R. A. (2008) Autophagy induction and autophagosome clearance in neurons: relationship to autophagic pathology in Alzheimer's disease. *J. Neurosci.* **28**, 6926-6937
  31. Nixon, R. A., Mathews, P. M., and Cataldo, A. M. (2001) The neuronal endosomal-lysosomal system in Alzheimer's disease. *J. Alzheimers. Dis.* **3**, 97-107
  32. Knauer, M. F., Soreghan, B., Burdick, D., Kosmoski, J., and Glabe, C. G. (1992) Intracellular accumulation and resistance to degradation of the Alzheimer amyloid A4/β protein. *Proc. Natl. Acad. Sci.* **89**, 7437-7441
  33. Peralvarez-Marin, A., Barth, A., and Graslund, A. (2008) Time-resolved infrared spectroscopy of pH-induced aggregation of the Alzheimer Aβ(1-28) peptide. *J. Mol. Biol.* **379**, 589-596
  34. Walsh, D. M., Klyubin, I., Fadeeva, J. V., Cullen, W. K., Anwyl, R., Wolfe, M. S., Rowan, M. J., and Selkoe, D. J. (2002) Naturally secreted oligomers of amyloid β protein potently inhibit hippocampal long-term potentiation in vivo. *Nature* **416**, 535-539
  35. Lacor, P. N., Buniel, M. C., Chang, L., Fernandez, S. J., Gong, Y., Viola, K. L., Lambert, M. P., Velasco, P. T., Bigio, E. H., Finch, C. E., Krafft, G. A., and Klein, W. L. (2004) Synaptic

- targeting by Alzheimer's-related amyloid  $\beta$  oligomers. *J. Neurosci.* **24**, 10191-10200
36. Cleary, J. P., Walsh, D. M., Hofmeister, J. J., Shankar, G. M., Kuskowski, M. A., Selkoe, D. J., and Ashe, K. H. (2005) Natural oligomers of the amyloid- $\beta$  protein specifically disrupt cognitive function. *Nat. Neurosci.* **8**, 79-84
  37. Balducci, C., Beeg, M., Stravalaci, M., Bastone, A., Scip, A., Biasini, E., Tapella, L., Colombo, L., Manzoni, C., Borsello, T., Chiesa, R., Gobbi, M., Salmona, M., and Forloni, G. (2010) Synthetic amyloid- $\beta$  oligomers impair long-term memory independently of cellular prion protein. *Proc. Natl. Acad. Sci.* **107**, 2295-2300
  38. Benilova, I., Karran, E., and De Strooper, B. (2012) The toxic A $\beta$  oligomer and Alzheimer's disease: an emperor in need of clothes. *Nat. Neurosci.* **15**, 349-357
  39. Liu, R. Q., Zhou, Q. H., Ji, S. R., Zhou, Q., Feng, D., Wu, Y., and Sui, S. F. (2010) Membrane localization of  $\beta$ -amyloid 1-42 in lysosomes: a possible mechanism for lysosome labilization. *J. Biol. Chem.* **285**, 19986-19996
  40. Yang, A. J., Chandswangbhuvana, D., Margol, L., and Glabe, C. G. (1998) Loss of endosomal/lysosomal membrane impermeability is an early event in amyloid A $\beta$ 1-42 pathogenesis. *J. Neurosci. Res.* **52**, 691-698
  41. Ditaranto, K., Tekirian, T. L., and Yang, A. J. (2001) Lysosomal membrane damage in soluble A $\beta$ -mediated cell death in Alzheimer's disease. *Neurobiol. Dis.* **8**, 19-31
  42. Cataldo, A. M., Barnett, J. L., Pieroni, C., and Nixon, R. A. (1997) Increased neuronal endocytosis and protease delivery to early endosomes in sporadic Alzheimer's disease: neuropathologic evidence for a mechanism of increased  $\beta$ -amyloidogenesis. *J. Neurosci.* **17**, 6142-6151
  43. Nixon, R. A., and Cataldo, A. M. (2006) Lysosomal system pathways: genes to neurodegeneration in Alzheimer's disease. *J. Alzheimers. Dis.* **9**, 277-289
  44. Lee, J. H., Yu, W. H., Kumar, A., Lee, S., Mohan, P. S., Peterhoff, C. M., Wolfe, D. M., Martinez-Vicente, M., Massey, A. C., Sovak, G., Uchiyama, Y., Westaway, D., Cuervo, A. M., and Nixon, R. A. (2010) Lysosomal proteolysis and autophagy require presenilin 1 and are disrupted by Alzheimer-related PS1 mutations. *Cell* **141**, 1146-1158

*Acknowledgments*—We thank Dr. Steve Caplan (University of Nebraska, NE) for providing the cDNA constructs for GFP-Rab5-WT, Rab5-DN and Rab5-CA, Dr. Wim Annaert (VIB Center for the Biology of Disease, Belgium) for providing the cDNA construct for GFP-Rab11-CA, and Dr. Yadong Huang (Gladstone Institutes, CA) for providing recombinant apoE3 and apoE4 proteins.

## FOOTNOTES

\*This work was supported by NIH grants R01AG027924, R01AG035355, P01AG030128, and P01 NS074969 (to G.B.), a grant from the Alzheimer's Association (to G.B.), and a NIH ADRC pilot grant P50AG16574 (to T.K.).

#The abbreviations used are: AD, Alzheimer's disease; A $\beta$ , amyloid- $\beta$ ; APP, amyloid precursor protein; apoE, apolipoprotein E; CA, constitutively active; DN, dominant-negative; ELISA, enzyme-linked immune-sorbent assay; FACS, fluorescence-activated cell sorter; HSPG, heparan sulphate proteoglycan; LDL, low-density lipoprotein; Tf, transferrin; WT, wild-type.

## FIGURE LEGENDS

**FIGURE 1.** A $\beta$ 42 traffics through Rab5-positive early endosomal compartments. A. N2a cells were transiently transfected with GFP vector (control), GFP-Rab5-WT, GFP-Rab5-DN or GFP-Rab5-CA, and incubated with TMR-A $\beta$ 42 (500 nM) for 24 h. Cells were observed by fluorescence confocal

microscopy and representative cells are shown. Inset shows a high-magnification view of A $\beta$ /Rab5 co-localization. Scale bar: 10  $\mu$ m. B. The percentages of A $\beta$  co-localized with Rab5 as of total A $\beta$  were quantified by ImageJ. Data are plotted as mean  $\pm$  SEM (n=9). C. N2a cells transiently transfected with the same set of constructs as in (A) were incubated with unlabeled A $\beta$ 42 (500 nM) for 24 h, and the amounts of cell-associated A $\beta$  were quantified by ELISA. Data are plotted as mean  $\pm$  SEM (n=3). *N.S.*, not significant; \*,  $p < 0.05$ . D. N2a cells transiently transfected with the same set of constructs as in (A) were incubated with Alexa568-conjugated Tf (20  $\mu$ g/ml) for 24 h. Cells were observed by fluorescence confocal microscopy with representative images shown. Scale bar: 10  $\mu$ m. E. The percentages of Tf co-localized with Rab5 as of total Tf were quantified by ImageJ. Data are plotted as mean  $\pm$  SEM (n=9).

**FIGURE 2.** A $\beta$ 42 traffics through Rab11-positive recycling endosomal compartments. A. N2a cells were transiently transfected with GFP vector (control), GFP-Rab11-WT, GFP-Rab11-DN or GFP-Rab11-CA, and incubated with TMR-A $\beta$ 42 (500 nM) for 24 h. Cells were observed by fluorescence confocal microscopy and representative cells are shown. Insets show high-magnification views of A $\beta$ /Rab11 co-localization. Scale bar: 10  $\mu$ m. B. The percentages of A $\beta$  co-localized with Rab11 as of total A $\beta$  were quantified by ImageJ. Data are plotted as mean  $\pm$  SEM (n=9). C. N2a cells transiently transfected with the same set of constructs as in (A) were incubated with native, unlabeled A $\beta$ 42 (500 nM) for 24 h, and the amounts of cell-associated A $\beta$  were quantified by ELISA. Data are plotted as mean  $\pm$  SEM (n=3). *N.S.*, not significant; \*,  $p < 0.05$ . D. N2a cells transiently transfected with the same set of constructs as in (A) were incubated with Alexa568-conjugated Tf (20  $\mu$ g/ml) for 24 h. Cells were observed by fluorescence confocal microscopy with representative images shown. Scale bar: 10  $\mu$ m. E. The percentages of Tf co-localized with Rab11 as of total Tf were quantified by ImageJ. Data are plotted as mean  $\pm$  SEM (n=9).

**FIGURE 3.** Co-localization of internalized A $\beta$ 42 with Rab5, Rab11, Rab7 and LAMP1 in primary neurons. Mouse primary cortical neurons were incubated with FAM-A $\beta$ 42 (500 nM) for 1 h (Rab5), 3 h (Rab11 and Rab7), or 24 h (LAMP1). Following immunostaining with antibodies to Rab5A (A), Rab11 (B), Rab7 (C), or LAMP1 (D), neurons were observed by fluorescence confocal microscopy with representative neuronal cell bodies and neurites shown. The panels to the right are high-magnification views of neurites from the white rectangle areas in the original images. Insets show high-magnification views of cell bodies from the white square areas in the original images. Scale bar: 10  $\mu$ m.

**FIGURE 4.** A $\beta$  degradation or aggregation in the lysosomes. A. N2a cells were transiently transfected with GFP vector (control), GFP-Rab5-WT, GFP-Rab7-WT or GFP-Rab11-WT, and incubated with A $\beta$ 42 (500 nM) in the presence or absence of lysosomal inhibitors (LI) for 24 h. The amounts of cell-associated A $\beta$  were quantified by ELISA. Data are plotted as mean  $\pm$  SEM (n=3). *N.S.*, not significant; \*,  $p < 0.05$ . B. N2a cells transfected and treated with A $\beta$ 42 as in (A) were homogenized and incubated with TMR-A $\beta$ 42 (100 nM) for 48 h. A $\beta$  aggregates were observed by fluorescence confocal microscopy with representative fields shown. Cells without A $\beta$  treatment were used as a negative control (a), and pre-formed A $\beta$  fibrils were used as a positive control (f). Scale bar: 20  $\mu$ m. C. The amounts of A $\beta$  aggregates were quantified by ImageJ software as shown as combined fluorescence intensity from 9 different fields of one chamber. Data are plotted as mean  $\pm$  SEM (n=3). *N.S.*, not significant, \*,  $p < 0.05$ .

**FIGURE 5.** ApoE facilitates cellular A $\beta$  uptake, lysosomal trafficking and degradation in an isoform-dependent manner. A. N2a cells were incubated with A $\beta$ 42 (500 nM), together with vehicle

control, apoE3 or apoE4 (500 nM) in the presence or absence of lysosomal inhibitors for 24 h, and the amounts of cell-associated A $\beta$  were quantified by ELISA. Data are plotted as mean  $\pm$  SEM (n=3). \*,  $p<0.05$ ; \*\*,  $p<0.01$ . B. The amounts of degraded A $\beta$  were calculated by subtracting the mean values of cell-associated A $\beta$  in the absence of inhibitors from the values in the presence of inhibitors. Data are plotted as mean  $\pm$  SEM (n=3). \*,  $p<0.05$ ; \*\*,  $p<0.01$ . C. Cells were incubated with FAM-A $\beta$ 42 (500 nM), together with vehicle control, apoE3 or apoE4 (500 nM) in the presence of lysosomal inhibitors for 24 h. LysoTracker Red (75 nM) was included in the final hour of incubation prior to processing for fluorescence microscopy. Scale bar: 10  $\mu$ m. D. The amounts of A $\beta$  co-localized with lysosomes were quantified by ImageJ. Data are plotted as mean  $\pm$  SEM (n=9). \*,  $p<0.05$ ; \*\*,  $p<0.01$ .

**FIGURE 6.** ApoE increases A $\beta$  cell surface binding to HSPG in an isoform-dependent manner. N2a cells were incubated with FAM-A $\beta$ 42 (2  $\mu$ M), together with vehicle control, apoE3 or apoE4 (500 nM) in the presence or absence of heparin (30 U/ml) at 4°C for 2 h. Cell-bound A $\beta$  was quantified by FACS. Data are plotted as mean  $\pm$  SEM (n=3). *N.S.*, not significant; \*,  $p<0.05$ ; \*\*,  $p<0.01$ .

**FIGURE 7.** ApoE3 lysosomal trafficking and degradation is more efficient than apoE4. A. N2a cells were prepared as in Fig. 5A, and the amounts of cell-associated apoE were quantified by ELISA. Data are plotted as mean  $\pm$  SEM (n=3). \*\*,  $p<0.01$ . B. The amounts of degraded apoE were calculated by subtracting the mean values of cell-associated apoE in the absence of inhibitors from the values in the presence of inhibitors. Data are plotted as mean  $\pm$  SEM (n=3). \*\*,  $p<0.01$ . C. Cells were incubated with A $\beta$ 42 (500 nM), together with vehicle control, apoE3 or apoE4 (500 nM) in the presence of lysosomal inhibitors for 24 hours, immunostained with antibodies against apoE and LAMP1 and observed by fluorescence confocal microscopy. Scale bar: 10  $\mu$ m. D. The amounts of apoE co-localizes with lysosomes were quantified by ImageJ. Data are plotted as mean  $\pm$  SEM (n=9). \*,  $p<0.05$ .

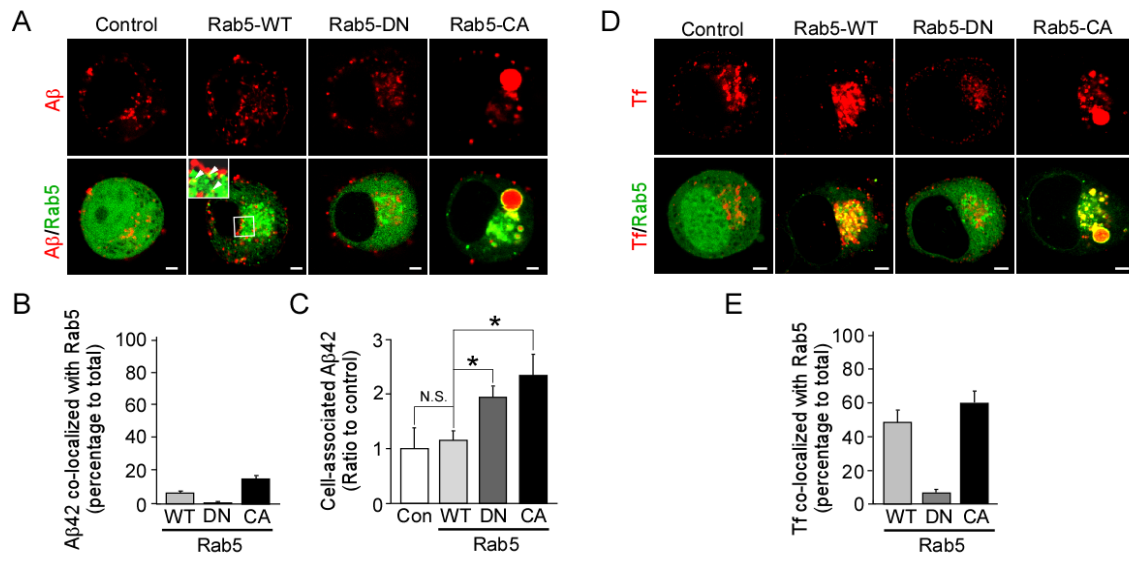


**Figure 1**

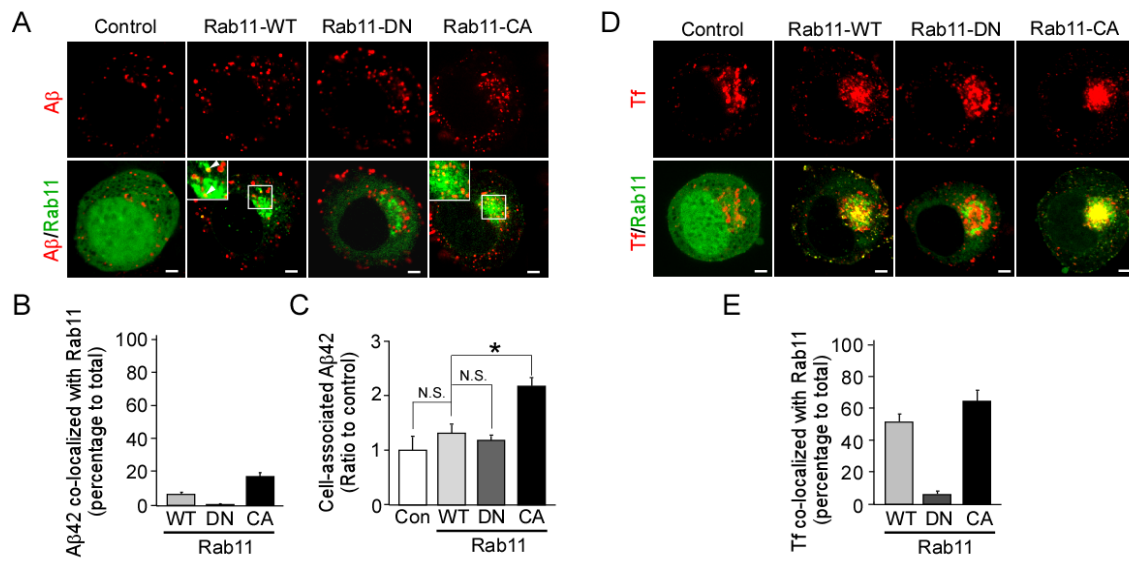


**Figure 2**

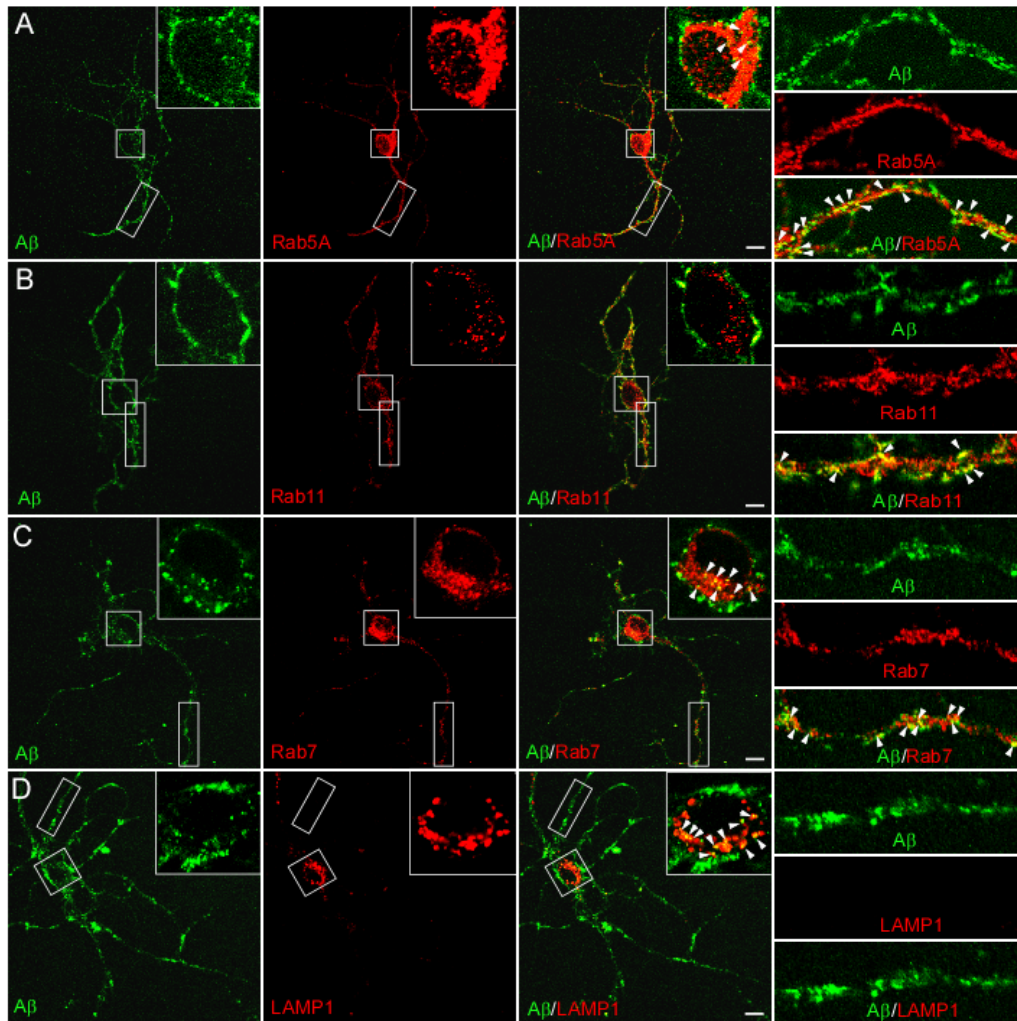


**Figure 3**

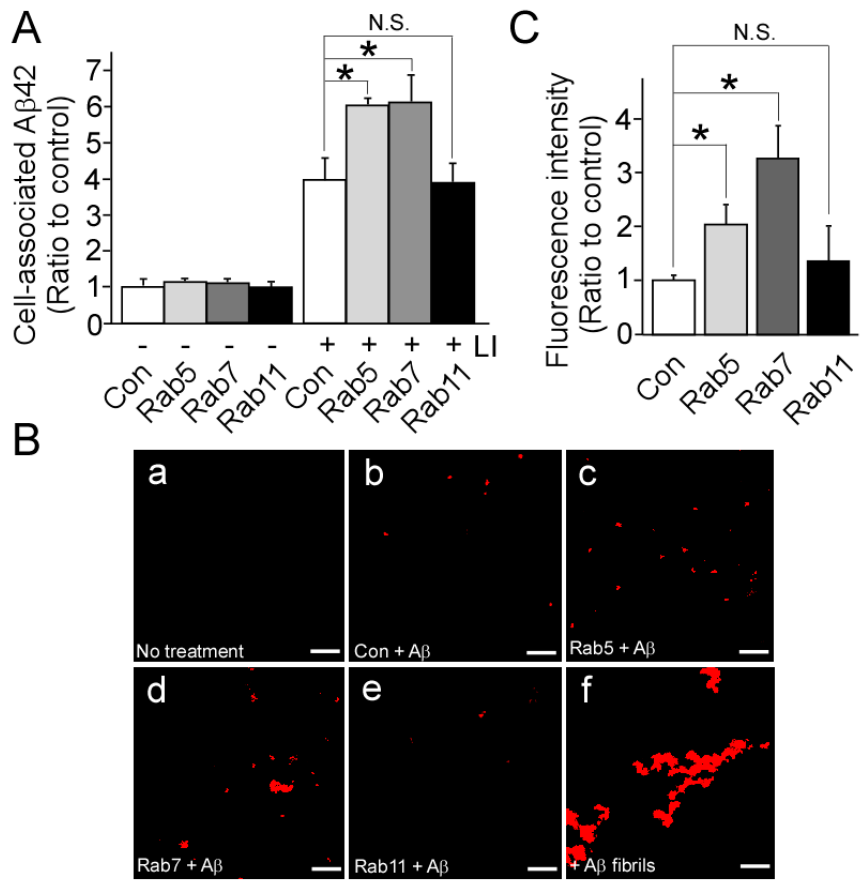


**Figure 4**

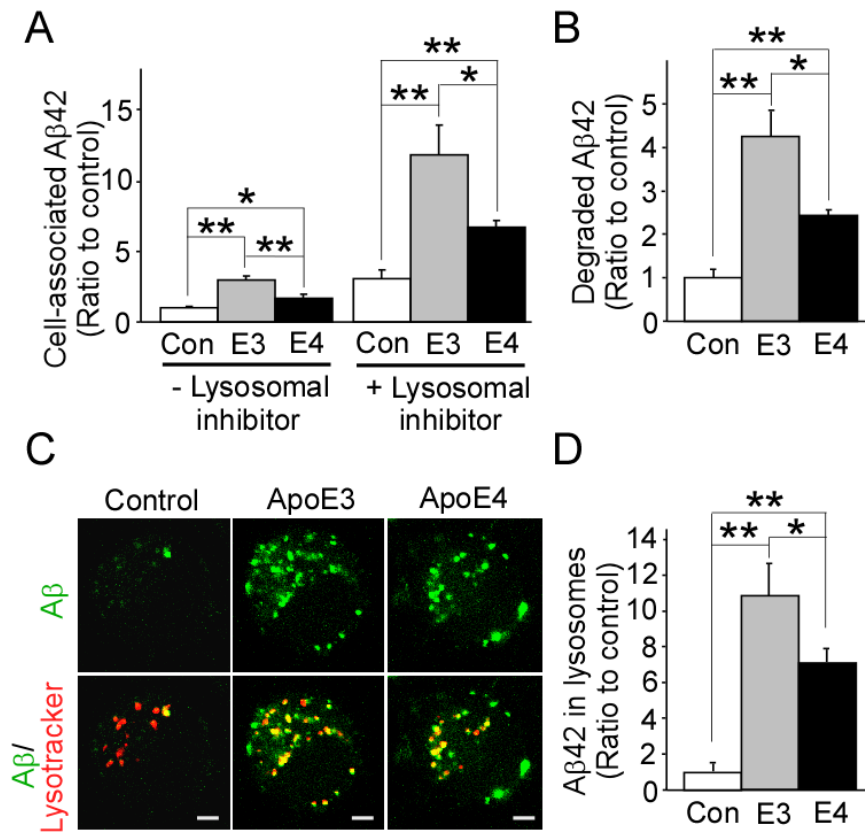


**Figure 5**

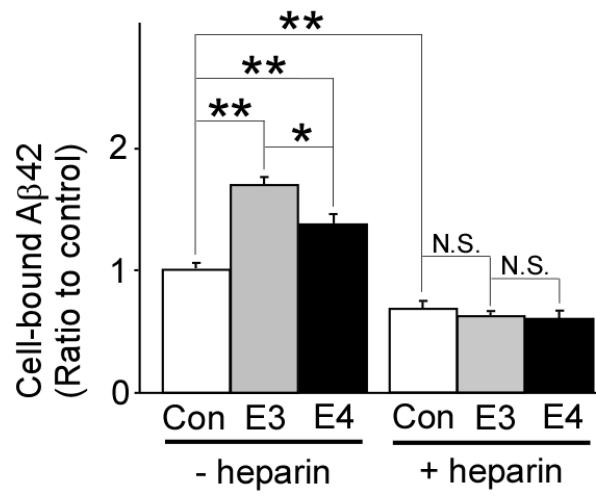


**Figure 6**

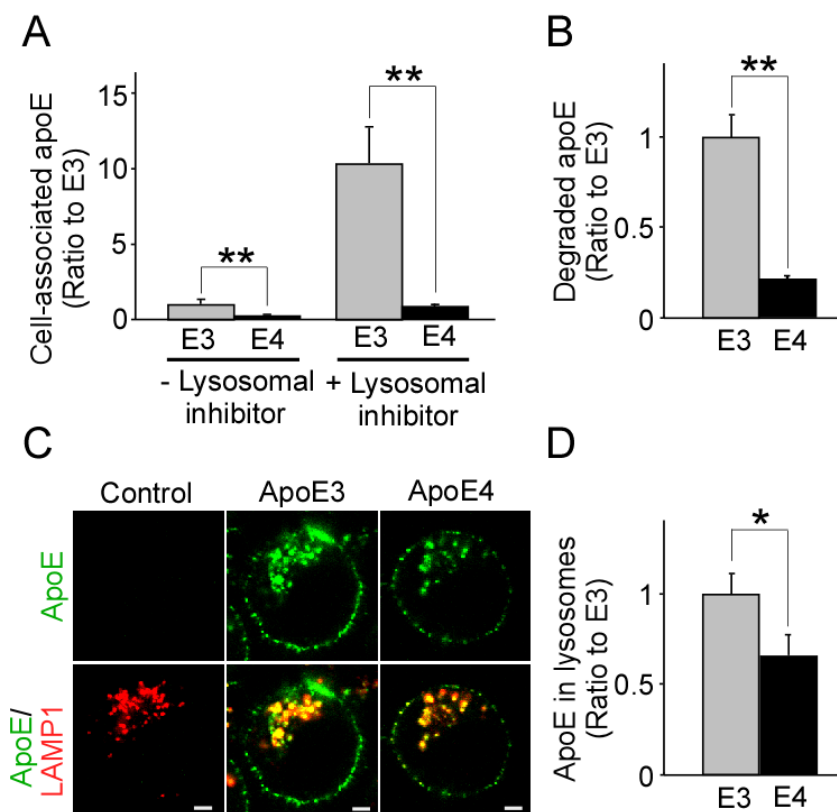


**Figure 7**